Monte Carlo simulations of continuum percolation of 3D well fluids

1990 J. Phys.: Condens. Matter 2 2241

(http://iopscience.iop.org/0953-8984/2/9/013)

J. Phys.: Condens. Matter 2 (1990) 2241–2249. Printed in the UK

Monte Carlo simulations of continuum percolation of 3D well fluids

D M Heyes

Department of Chemistry, Royal Holloway and Bedford New College, University of London, Egham, Surrey TW20 OEX, UK

Received 16 November 1989

Abstract. We investigate the percolation threshold, ρ_p, of three-dimensional continuum attractive and repulsive square-well, triangular-well and parabolic-well fluids by Monte Carlo computer simulation. We find that in the hard-core limit an attractive well decreases ρ_p below the high-temperature limiting value. In contrast a hard shoulder potential produces the opposite trend. We quantify the role of the range and shape of the well potential in determining the value of the percolation threshold. We examine the shapes of all the clusters at the percolation threshold, resolved as a function of the number of particles in a cluster, s. The asphericity parameter, A_3, describing the instantaneous shape of the cluster, decays slowly from unity, achieving $\simeq 0.3$ by $s \simeq 70$, statistically indistinguishable from the estimated universal value of 0.312 for percolation clusters.

1. Introduction

The concept of percolation, i.e., the formation of an infinitely ranged pathway through space, has found many applications in chemical physics. For example, it provides a starting point for modelling the physical properties of colloidal dispersions as they aggregate or undergo a sol/gel transition. We continue our exploration of the effect of the form and range of the molecular pair potential on the value of the percolation threshold for continuum fluids. We consider the generic hard-core 'well' molecules. These model molecules interact here via a square-, triangular- or parabolic-well pair potential where the potential minimum or shoulder has a strength of $\sim k_B T$. The motivation for this study lies ultimately in understanding colloid particle stabilisation applied by a surface coating. A wide variety of coatings can be idealised by these potential forms. Polymer stabilised colloids would be close to a hard-sphere potential with a thin repulsive shoulder, of an analytic form depending on the chemistry of the adsorbate. Similarly surface charged colloids can have a thin attractive layer around the hard repulsive core. We are interested in how the nature of the coating will affect the long-range order of the particles. We have idealised these into three well types, illustrated in figure 1, to cover a range of degrees of interpenetration between the 'adsorbed' layers. Interest to date in applying percolation concepts to study colloids and microemulsions has been dominated by the calculation of the scaling exponents. In this work we concentrate rather on the value of the percolation threshold.

Despite there being a long-standing interest in analytic treatments of continuum percolation and the 'pair connectedness' (Hill 1955, Coniglio *et al* 1977) it is only in the last few years that simulation has been used to focus attention on quantifiable results

0953-8984/90/092241+09$03.50

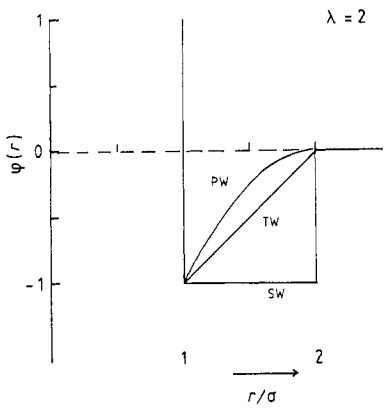

Figure 1. The potentials used in the simulations. Key: SW, equation (7); TW, equation (8); PW, equation (9). We show the $\varphi(r)$ for the attractive wells with $\lambda = 2$. The repulsive well or shoulder potentials are obtained by inverting the $\varphi(r)$ for $\sigma < r < \lambda\sigma$ about the abscissa.

for specific pair potentials. There has already been considerable interest in continuum percolation of spherical particles by MC. Randomly centred spheres, where there is no hindrance to overlap, have been considered (Balberg 1988). Partially penetrable hard core spheres, (Lee and Torquato 1988) and attractive square wells (Chiew and Wang 1988) have also been investigated. As with previous studies we limit our interest to the case where the connectivity distance, σ_s, equals the range of the potential up to where $\varphi(r) = 0$. By carrying out an N-dependence study, Metropolis Monte Carlo computer simulation is shown here to give an accurate value for the percolation threshold, ρ_p to within several per cent, using only several hundred particles in the simulation cell. (The percolation exponents themselves are difficult to obtain accurately with these system sizes to better than ± 0.05.) We are particularly interested in discovering the effect of an attractive and repulsive shoulder to the hard-core centre. In previous reports (Heyes and Melrose 1988, 1989a), the percolation cluster statistics of the 3D Lennard-Jones (LJ) fluid were described. We have also investigated the corresponding 2D fluid by MD (Cooper *et al* 1989) and the 2D square-well, SW, fluid by MC (Heyes and Melrose 1989b).

2. Monte Carlo simulations

Our method of determining clusters is identical to that used previously (Heyes and Melrose 1988). We consider partially permeable spheres (or 'soft shells') of diameter σ_s centred on those of the hard cores. Particles are connected if their soft shells overlap. Percolation occurs when a connected cluster spans the infinite replica system. As σ_s diminishes, (i.e., the so-called soft-core–hard-core transition) the repulsive core and attractive outer zone of the particle influences the nature of the clusters formed out of the soft shells and thereby affects the percolation characteristics. The next step forward of these continuum percolation studies is that we explore the interplay between the underlying phase behaviour of these fluids and the long-range order.

We evaluated the function, P, the fraction of configurations generated by the computer that manifested at least one percolating cluster (PC). The percolation threshold in the thermodynamic limit (i.e., $N \to \infty$), ρ_p, is best estimated for finite N when $P = 0.5$, because it shows the smallest system-size (i.e., N) dependence.

The distribution of different sized clusters is characterised by the cluster number distribution function, n_s, which for these continuum ('off-lattice') systems is the time-average number of clusters containing s particles, N_s divided by N i.e., $n_s = N_s/N$

(Balberg and Binenbaum 1985). At the percolation threshold

$$n_s(\rho_p) \sim s^{-\tau} \qquad s \to \infty. \tag{1}$$

For finite periodic systems there is an upper bound on s, i.e., $1 \leq s \leq N$, resulting in distortions from (1) for $s \to N$.

At the percolation threshold, the radius of gyration, R_g, provides a route to the fractal dimension, D_f of the non-percolating clusters.

$$R_g = \left\langle \frac{1}{2} \sum_{i}^{s-1} \sum_{j \neq i}^{s} R_{ij}^2 / s(s-1) \right\rangle^{1/2}. \tag{2}$$

where $\boldsymbol{R}_{ij}$ is the vector separation between particles i and j. The scaling relationship here is $R_g \sim s^{1/D_f}$ as $s \to \infty$.

The pair radial distribution function, $g(r)$ and pair connectedness function, $p(r)$, for pair separations, r, are probes of the local structure in the whole fluid and within the clusters, respectively

$$g(r) = n(r)/4\pi r^2 \rho\, \delta r \tag{3}$$

where δr is the radial increment for $n(r)$; $n(r)$ is the number of particles found on average within $r - \delta r/2 \leq r \leq r + \delta r/2$.

If P_∞ is the fraction of molecules in the percolating cluster, PC, then at ρ_p

$$p(r) = n(r)' P_\infty / 4\pi r^2 \rho\, \delta r \tag{4}$$

where $n(r)'$ is the number of particles found on average within $r - \delta r/2 \leq r \leq r + \delta r/2$ within the same cluster. (All clusters are used for this, not just the PC) As $r \to \infty$ then $p(r) \to P_\infty^2$. Therefore, the $p(r)$ looks similar to $g(r)$ at short range but attains a lower limiting value when the pair separation becomes comparable to the size of the periodic cell. In the limit $r \to \infty$, $p(r) \sim r^{D_f - 3}$. In practice, we found that D_f is obtained more accurately from the function

$$m(r) = \int_0^r n(r')\, \mathrm{d}r' \tag{5}$$

which has the limiting value r^{D_f} for large r.

A new feature of this work is the determination of the shape of the clusters (Bishop and Clarke 1989). We measure the instantaneous shape of the clusters, as a function of s. The shape of the cluster is determined from its tensor components of the radius of gyration. The trace of this is equal to R_g^2 and the eigenvalues, λ_i, are the components of R_g^2 along the principal orthogonal axes. In dimension, d, the asphericity, A_d, of the cluster is measured by [24]

$$A_d = \frac{\Sigma_{i>j}^{d} \langle (\lambda_i - \lambda_j)^2 \rangle}{(d-1) \langle (\Sigma_{i=1}^{d} \lambda_i)^2 \rangle}. \tag{6}$$

If the cluster is highly symmetric, roughly spherical, then $A_d \to 0$, whereas if it is rod-shaped, then $A_d = 1$.

3. Simulation details

The MC calculations were performed on cubic unit cells of volume V containing $N = 256$ and $N = 500$ hard-core particles. The Metropolis MC technique was used for particles interacting via the following pair potentials:

(i) square well:

$$\varphi(r) = \begin{cases} \infty & r \leq \sigma \\ -\varepsilon & \sigma < r \leq \lambda\sigma \\ 0 & r > \lambda\sigma \end{cases} \tag{7}$$

(ii) triangular well:

$$\varphi(r) = \begin{cases} \infty & r \leq \sigma \\ -\varepsilon(\lambda\sigma - r)/(\lambda\sigma - \sigma) & \sigma < r \leq \lambda\sigma \\ 0 & r > \lambda\sigma \end{cases} \tag{8}$$

(iii) parabolic well:

$$\varphi(r) = \begin{cases} \infty & r \leq \sigma \\ -\varepsilon(\lambda\sigma - r)^2/(\lambda\sigma - \sigma)^2 & \sigma < r \leq \lambda\sigma \\ 0 & r > \lambda\sigma. \end{cases} \tag{9}$$

For brevity we denote these the SW, TW and PW pair-potentials respectively. The hard-core diameter of the particles is σ. For attractive wells, $\varepsilon = 1$, and for repulsive 'well' or shoulder particles, $\varepsilon = -1$. We use

$$\sigma_s = \lambda\sigma. \tag{10}$$

It is not necessary for the 'capture' radius and potential range to coincide. The cases where $\sigma_s \neq \lambda\sigma$ could be studied also. The simulations were for ~ 8000 attempted moves per particle for $N = 256$ and for ~ 4000 attempted moves per particle for $N = 500$. The maximum displacement distance per particle was periodically adjusted during the simulation in order achieve a move acceptance fraction of 0.5. We employ the following reduced units throughout, i.e., $k_B T/\varepsilon \rightarrow T$, and number density, $\rho = N\sigma^3/V$.

4. Results and discussion

In table 1 we present a summary of the values for ρ_p attained by the MC simulations for the attractive well potentials. In figure 2 the boundary lines between percolating and non-percolating states for a selection of σ_s are given. A range of σ_s is considered, which spans essentially the whole of the phase diagrams for these three fluids. In the hard-core limit (e.g., $\sigma_s \lesssim 1.5$), the value of ρ_p decreases with fall in temperature from $T = 10 \rightarrow 0.5$, the range considered here. The effect is most pronounced in the ascending order, PW, TW and SW. The ρ_p manifest a curvature to *lower* density as T decreases. The $\sigma_s \geq 2.0$ lines increasingly show a ρ_p that shift towards *higher* density as temperature decreases. The effect is pronounced at $\sigma_s = 3.0$ for example. This behaviour is also obtained in 2D (Bug *et al* 1985). The N dependence of these ρ_p, as given in table 1, is only a few per cent for $T \sim 10$.

Table 1. The percolation thresholds of the triangular-well (TW) and parabolic-well (PW) potential fluids. The simulation parameters and properties. Key: T, reduced temperature; N, number of molecules in the MC cell; ρ_p, percolation threshold reduced number density; Φ/Nk_BT, average potential energy per particle divided by thermal energy; $g(\sigma_+)$, value of $g(r)$ at $r = \sigma + \delta$, $\delta > 0, \rightarrow 0$. Similarly, $g(\sigma_{\lambda-})$ is $g(r)$ at $r = \lambda\sigma - \delta$ and $g(\sigma_{\lambda+})$ is $g(r)$ at $r = \lambda\sigma + \delta$. $P/\rho_B T$, usual compressibility factor.

T	N		σ_s	ρ_p	Φ/Nk_BT	$g(\sigma_+)$	$g(\sigma_{\lambda-})$	$g(\sigma_{\lambda+})$	$P/\rho k_BT$
10.0	500	TW	1.1	0.564	−0.033	2.61	1.81	1.80	2.01
2.0	500	TW	1.1	0.531	−0.197	3.30	1.60	1.59	3.18
1.0	500	TW	1.1	0.489	−0.492	4.31	1.42	1.39	2.38
0.75	500	TW	1.1	0.462	−0.611	5.39	1.26	1.28	2.00
0.5	500	TW	1.1	0.395	−0.515	8.53	1.08	1.11	1.32
10.0	500	TW	1.2	0.381	−0.039	1.83	1.30	1.31	2.30
2.0	500	TW	1.2	0.359	−0.231	2.42	1.19	1.20	1.97
1.0	500	TW	1.2	0.333	−0.511	3.23	1.07	1.06	1.48
0.5	500	TW	1.2	0.266	−0.981	6.52	0.87	0.87	0.69
10.0	256	TW	1.5	0.178	−0.046	1.44	1.02	1.04	1.45
2.0	256	TW	1.5	0.171	−0.256	1.73	0.97	0.94	1.18
0.75	256	TW	1.5	0.147	−0.916	3.56	0.91	0.89	0.74
0.5	256	TW	1.5	0.123	−2.726	10.93	1.31	1.24	0.30
10.0	500	TW	1.5	0.177	−0.045	1.35	1.03	1.03	1.42
2.0	500	TW	1.5	0.174	−0.262	1.84	0.96	0.96	1.20
0.75	500	TW	1.5	0.150	−0.964	1.93	0.94	0.94	0.66
0.5	500	TW	1.5	0.131	−2.284	10.46	1.23	1.23	0.12
10.0	500	TW	3.0	0.0218	−0.042	1.04	0.96	0.97	1.00
2.0	500	TW	3.0	0.0236	−0.262	1.38	0.96	0.95	0.80
0.75	500	TW	3.0	0.0752	−10.06	33.31	2.17	2.12	−1.25
0.5	500	TW	3.0	0.0943	−19.85	57.35	2.21	2.17	−2.71
14.0	500	PW	1.05	0.753	−0.010	3.83	2.80	2.71	6.63
10.0	500	PW	1.05	0.750	−0.021	3.77	2.78	2.74	6.36
2.0	500	PW	1.05	0.728	−0.154	5.04	2.56	2.50	5.63
0.75	500	PW	1.05	0.678	−0.535	8.39	1.97	2.12	3.23
0.5	500	PW	1.05	0.638	−0.972	12.53	1.62	1.73	0.72
10.0	500	PW	1.1	0.561	−0.031	2.57	1.82	1.81	3.72
4.0	500	PW	1.1	0.549	−0.083	2.79	1.75	1.74	3.46
0.75	500	PW	1.1	0.468	−0.746	5.53	1.27	1.27	2.10
0.5	500	PW	1.1	0.393	−1.297	8.81	1.10	1.14	1.36
10.0	500	PW	1.2	0.385	−0.027	1.88	1.34	1.31	2.36
4.0	500	PW	1.2	0.377	−0.051	2.11	1.30	1.31	2.25
0.75	500	PW	1.2	0.342	−0.522	4.69	1.08	1.07	1.58
0.5	500	PW	1.2	0.312	−1.069	7.51	0.94	0.99	1.03
10.0	256	PW	1.5	0.180	−0.025	1.37	1.01	1.04	1.44
4.0	256	PW	1.5	0.177	−0.076	1.56	1.00	1.01	1.39
0.75	256	PW	1.5	0.166	−0.619	3.62	0.90	0.93	0.92
0.5	256	PW	1.5	0.150	−1.290	7.34	0.95	0.95	0.61
0.3	256	PW	1.5	0.142	−5.525	27.7	0.95	0.98	−0.48
10.0	500	PW	3.0	0.022	−0.043	1.18	0.98	0.98	1.01
4.0	500	PW	3.0	0.022	−0.118	1.41	0.98	0.98	0.94
0.75	500	PW	3.0	0.085	−11.90	37.74	2.44	2.43	−1.43
10.0	500	PW	3.0	0.025	−0.005	0.59	0.96	0.97	1.01
4.0	500	PW	3.0	0.024	−0.066	1.35	1.02	1.00	0.99
0.75	500	PW	3.0	0.026	−0.928	6.13	1.06	1.09	0.50
0.50	500	PW	3.0	0.046	−7.086	42.95	1.73	1.73	−0.54

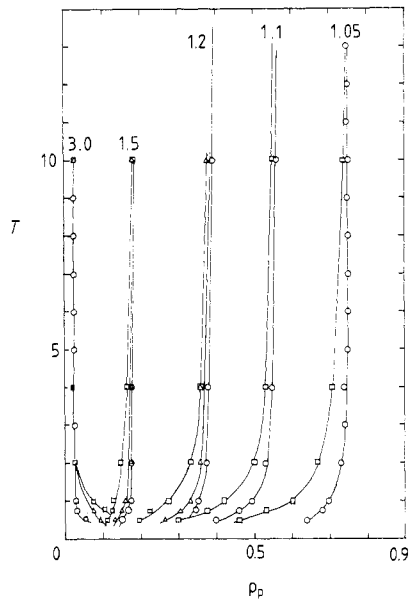

Figure 2. The percolation thresholds for the 3D SW, TW and PW fluids. The full curves denote boundaries between non-percolating states (to the left) and percolating states (to the right) of the line based on the MC computations. Key: SW, □; TW, △; PW, ○. Distance is in hard-core σ. Each line corresponds to and is annotated at the top of the figure with the relevant search diameter $\sigma_s = \lambda$ in hard-core units or σ units.

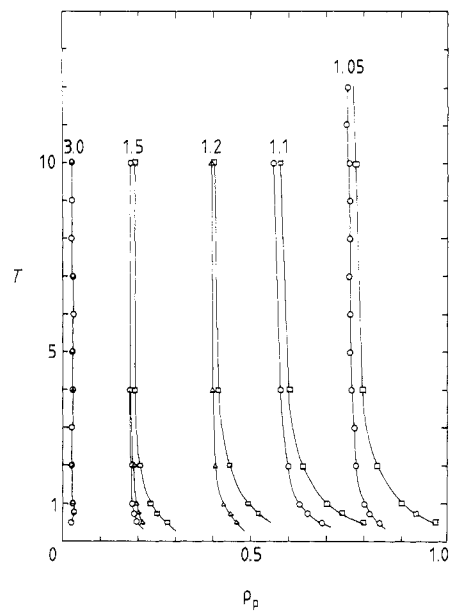

Figure 3. As for figure 2, except that the corresponding curves for the repulsive shoulder fluids are given.

We now consider the inverted well or 'shoulder' potential fluids. In table 2 we present a summary of the values for ρ_p attained by the MC simulations for the shoulder potentials. In figure 3 we show some representative percolation threshold curves for these fluids. As temperature drops the ρ_p increase at all λ-values, revealed in table 2 and figure 3 for selected λ. The effect is most pronounced in the ascending order PW, TW, SW. As there is no liquid–gas coexistence region produced by these repulsive potentials, we do not observe any anomalous trends in ρ_p as we vary σ_s or equivalently λ at $T \simeq 1$.

The difference in behaviour between square wells and square shoulder potentials is understood as follows. As temperature decreases the attractive square wells cause the network in the hard-core limit to become more 'fibrous' in appearance. Neighbours are attracted within the well range in order to reduce the energy of the system. Therefore a lower density of particles is required to induce percolation. (The soft-core limit proves to be an exception to this rule, as explained previously (Bug *et al* 1985).) The PW and TW have a smaller effective potential range than the SW particles with the same nominal well range, evident in figure 1. Therefore these particles exhibit a less extreme curvature of ρ_p in this temperature region. The reverse occurs for the 'shoulder' potentials. The decrease in temperature causes particles to depart from the region of radius λ about each particle. As the local connectivity is reduced, a higher density is required to induce percolation.

Table 2. As for table 1, except that the triangular and parabolic repulsive shoulder potential fluids are considered.

T	N		σ_s	ρ_p	Φ/Nk_BT	$g(\sigma_+)$	$g(\sigma_{\lambda-})$	$g(\sigma_{\lambda+})$	$P/\rho k_BT$
10.0	500	TW	1.1	0.575	0.052	2.28	1.91	1.90	4.04
1.0	500	TW	1.1	0.631	0.451	1.34	2.43	2.46	5.62
0.75	500	TW	1.1	0.650	0.496	1.10	2.64	2.65	6.30
0.5	500	TW	1.1	0.688	0.661	0.74	3.14	3.11	7.82
10.0	500	TW	1.2	0.389	0.050	1.65	1.38	1.37	2.51
2.0	500	TW	1.2	0.409	0.223	1.26	1.51	1.51	2.89
0.75	500	TW	1.2	0.445	0.511	0.81	1.81	1.82	3.90
0.5	500	TW	1.2	0.466	0.628	0.51	2.06	2.08	4.61
10.0	256	TW	1.5	0.183	0.047	1.16	1.06	1.07	1.53
2.0	256	TW	1.5	0.188	0.217	0.94	1.14	1.13	1.79
0.75	256	TW	1.5	0.202	0.458	0.55	1.31	1.28	2.30
0.5	256	TW	1.5	0.213	0.614	0.39	1.42	1.44	2.76
12.0	500	PW	1.05	0.758	0.061	3.18	2.85	2.86	6.50
10.0	500	PW	1.05	0.764	0.066	3.05	2.90	2.87	6.41
4.0	500	PW	1.05	0.770	0.070	3.01	2.97	2.93	7.18
1.0	500	PW	1.05	0.806	0.231	1.74	3.53	3.37	8.64
0.75	500	PW	1.05	0.815	0.264	1.31	3.73	3.60	9.14
0.50	500	PW	1.05	0.840	0.336	0.69	4.17	3.96	10.24
10.0	500	PW	1.1	0.562	0.050	2.24	1.88	1.88	3.92
2.0	500	PW	1.1	0.601	0.244	1.78	2.13	2.13	4.68
0.75	500	PW	1.1	0.649	0.486	1.07	2.59	2.64	6.23
10.0	500	PW	1.2	0.382	0.034	1.63	1.36	1.36	2.45
2.0	500	PW	1.2	0.399	0.151	1.21	1.45	1.44	2.74
0.75	500	PW	1.2	0.418	0.302	0.62	1.63	1.61	3.22
0.5	500	PW	1.2	0.434	0.400	0.38	1.77	1.76	3.65
10.0	256	PW	1.5	0.182	0.029	1.21	1.04	1.04	1.53
4.0	256	PW	1.5	0.183	0.072	1.09	1.07	1.06	1.59
2.0	256	PW	1.5	0.185	0.130	0.87	1.10	1.10	1.67
1.0	256	PW	1.5	0.185	0.231	0.62	1.14	1.13	1.84
0.75	256	PW	1.5	0.194	0.281	0.44	1.19	1.19	1.95
0.5	256	PW	1.5	0.196	0.347	0.29	1.22	1.24	2.18
9.0	500	PW	3.0	0.024	0.026	1.03	1.02	1.03	1.08
4.0	500	PW	3.0	0.024	0.058	0.79	1.00	1.01	1.11
1.0	500	PW	3.0	0.022	0.161	0.37	1.02	1.05	1.24
0.50	500	PW	3.0	0.023	0.253	0.16	1.06	1.08	1.42

In figure 4 we show the asymmetry parameter, A_3, for representative TW and PW state points at the percolation threshold. We note that for the non-percolating clusters A_3 decreases from 1 at $s = 2$ to $A_3 \simeq 0.5$ at $s = 5$. The overall trend, above the statistical fluctuations, reveals that the subsequent decrease is slow, i.e., $A_3 \simeq 0.3$ for $s \sim 70$, statistically the same as the interdimensional expansion prediction of $A_3 = 0.312$ for percolation clusters (Rudnick and Gaspari 1987). We expect that the A_3 of these large s clusters in the plateau region of figure 4 to be the same as the percolating cluster.

The cluster number distribution function, $n_s(s)$, has the exponent $\tau = 2.2$ on a 3D lattice (Stauffer 1985). We find that in the fluid phase the measured exponent τ' is slightly less than this value: $\tau' = 2.1 \pm 0.1$. (We use the notation τ' rather than τ here because τ is defined as the exponent of n_s in the asymptotic limit of $N \to \infty$.)

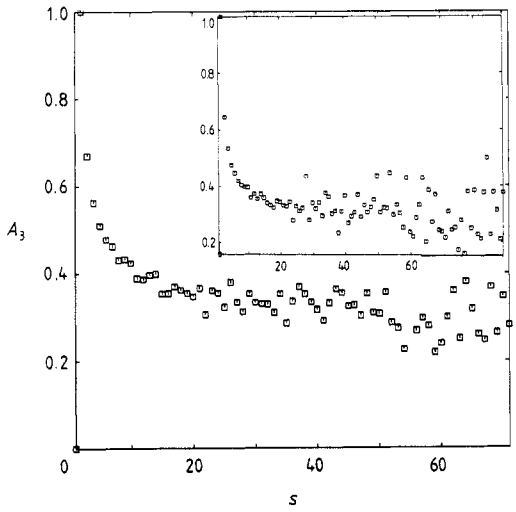

Figure 4. The asphericity parameter, A_3, from (6) for state points $\rho = 0.1849$, $T = 4$, $\lambda = 1.5$, $N = 256$, repulsive TW. Inset: $\rho = 0.6323$, $T = 1$, $\lambda = 1.1$, $N = 500$, repulsive PW.

We expect that for much larger systems (at present beyond the scope of molecular simulation) the evaluated τ' will increase to the universal value, that is $\tau' \rightarrow \tau$.

The non-percolating and percolating clusters formed from non-interacting particles on a lattice at ρ_p manifest the same fractal dimension, D_f. For non-interacting particles, percolation theory gives $D_f = d - \beta/\nu$, where d is the dimension of the space (= 3 here) and β and ν are the universal percolation exponents. In 3D, $\beta = 0.4$ and $\nu = 0.9$ (Stauffer 1985), $D_f = 2.5$. The extracted D_f of the percolating cluster from (5) gives $D_f = 2.7 \pm 0.1$, which again shows some deviation from the universal value, attributed to the small periodic systems considered here.

5. Conclusions

We have mapped out the percolation threshold curves of attractive well and repulsive shoulder potentials of three shapes. We have shown that the percolation threshold of these two classes of potential move in the opposite direction as a result of a temperature change. The attractive square-well potential fluids percolate at a lower density (in the hard-core limit) than the triangular-well or parabolic-well potential fluids. The opposite trend is observed in the soft-core limit.

The square-shoulder potential fluids percolate at a higher density (in the hard-core limit) than the triangular well or parabolic well potential fluids. As there is no liquid–vapour coexistence in any of the shoulder fluids, the percolation curves are more featureless than the equivalent well curves. We have also investigated the shapes of the clusters and found that, with no noticeable sensitivity to the connectivity distance, σ_s, or to the form of the potential, there is a slow loss of asphericity with increasing number of particles in the cluster. After a sharp reduction in asphericity for clusters up to about 10 particles in size, the subsequent approach to an asymptotic universal shape would appear to require ~ 70 particles.

In this work we have investigated the dependence of the percolation threshold on 'generic' pair potentials. In future work it would be of interest to relate the percolation properties of *specific* experimental colloidal systems with realistic interaction potentials.

Acknowledgments

DMH gratefully thanks the Royal Society for the award of a Royal Society 1983 University Research Fellowship and expresses gratitude to the SERC for the award of computer time on the CRAY-XMP at the University of London Computer Centre, and the RHBNC Computer Centre for use of their computing facilities. A referee is thanked for helpful comments.

References

Balberg I 1988 *Phys. Rev.* B **37** 2391
Balberg I and Binenbaum N 1985 *Phys. Rev.* A **31** 1222
Bishop M and Clarke J H R 1989 *J. Chem. Phys.* **90** 6647
Bug A L R, Safran S A, Grest G S and Webman I 1985 *Phys. Rev. Lett.* **55** 1896
Chiew Y C and Wang Y H 1988 *J. Chem. Phys.* **89** 6385
Coniglio A, De Angelis U and Forlani A 1977 *J. Phys. A: Math. Gen.* **10** 1123
Cooper N, Tedder A, Heyes D M and Melrose J R 1989 *J. Phys.: Condens. Matter* **1** 6217
Heyes D M and Melrose J R 1988 *J. Phys. A.: Math. Gen.* **21** 4075
—— 1989a *Mol. Phys.* **66** 1057
—— 1989b *Mol. Phys.* **68** 359
Hill T L 1955 *J. Chem. Phys.* **23** 617
Lee S B and Torquato S 1988 *J. Chem. Phys.* **89** 6427
Rudnick J and Gaspari G 1987 *Science* **237** 384
Stauffer D 1985 *Introduction to Percolation Theory* (London: Taylor and Francis) p 52